



# Sediment export in marly badland catchments modulated by frost-cracking intensity, Draix-Bléone Critical Zone Observatory, SE France.

Coline Ariagno<sup>1</sup>, Caroline Le Bouteiller<sup>1</sup>, Peter van der Beek<sup>2</sup> and Sébastien Klotz<sup>1</sup>

5 <sup>1</sup>Univ. Grenoble Alpes, INRAE, UR ETNA, Grenoble, France

<sup>2</sup>Institut für Geowissenschaften, Universität Potsdam, Germany

*Correspondence to:* Coline Ariagno (coline.ariagno@inrae.fr)

**Abstract.** At the interface between the lithosphere and the atmosphere, the critical zone records the complex interactions between erosion, climate, geologic substrate and life, and can be directly monitored. Long data records collected in the sparsely  
10 vegetated, steep marly badland catchments of the Draix-Bléone Critical Zone Observatory (CZO), SE France, allow analysing potential climatic controls on long-term regolith dynamics and sediment export. Although widely accepted as a first-order control, rainfall variability does not fully explain the observed inter-annual variability in sediment export, suggesting that regolith production and its controls may modulate the observed pattern of sediment export. Here, we define sediment-export anomalies as the residuals from a predictive model with annual rainfall intensity above a threshold as the control. We then use  
15 continuous soil-temperature data, recorded at different locations over multiple years, to highlight the role of frost weathering in regolith production. Several proxies for different frost-weathering processes have been calculated from these data and compared to the sediment-export anomalies, with careful consideration of field data quality. Our results suggest that frost-cracking intensity (linked to ice segregation) can explain about half (47-64%) of the sediment-export anomalies. In contrast, the number of freeze-thaw cycles (linked to volumetric expansion) has only a minor impact on catchment sediment response.  
20 The time spent below 0 °C also correlates well with the sediment-export anomalies and requires fewer field data to be calculated than the frost-cracking intensity. Thus, frost-weathering processes modulate sediment export by controlling regolith production in these catchments and should be taken into account when building a predictive model of sediment export from these badlands under a changing climate.

## 1. Introduction

25 Landscape erosion and its associated hazards, such as torrential floods, rockfalls, etc., are some of the visible consequences of the complex interaction between the Critical Zone and climate (e.g., Anderson et al., 2012). Regolith production is the result of a variety of processes, many of which are influenced by climate, and constitutes a critical first step in the source-to-sink sediment pathway (e.g. Dixon et al., 2009; Riebe et al., 2017). However, the impact of climate (change) on regolith production



and ensuing landscape erosion remains difficult to quantify. In a context of rapid global climate change, how will sediment  
30 production be influenced by climate change (e.g., Nearing et al., 2004; Hirschberg et al., 2021; Nadal-Romero et al., 2021)?  
How will dominant erosion processes evolve according to lithologies and climatic variations? How will vegetation evolve  
locally and will it amplify or reduce surface erosion? These questions, among others, motivate the study of soil weathering  
mechanisms and their sensitivity to climate (e.g., Nadal-Romero et al., 2018).

In badland areas, the interaction between erosion and climate is enhanced because of the absence of vegetation and the easily  
35 erodible lithology. Following the general definition, “badlands” refers to “deeply dissected erosional landscapes, formed in  
soft-rock terrain, commonly but not exclusively in semi-arid regions and with sparse vegetation, that have a high drainage  
density of rill and gully systems and are dominated by overland flow” (Harvey, 2004). The widespread badland landscapes  
known as “Terres Noires” in the South-Eastern French Alps have been extensively studied because of their susceptibility to  
erosion, leading to high sediment export (e.g., Antoine et al., 1995). Over the last 35 years, several small catchments in these  
40 marly badlands have been monitored in the framework of the Draix–Bléone Critical-Zone Observatory (CZO), leading to a  
quantification of weathering and erosion through repeated measurements of sediment yield at the event scale (Mathys et al.,  
2003). Because of the ample availability of sediment and the efficient network connectivity (Jantzi et al., 2017), floods in these  
catchments can transport a very large quantity of sediment (Delannoy and Rovéra, 1996). Such sediment-laden floods can  
potentially cause significant damage to downstream infrastructure. Landscape changes are easily and rapidly observable in the  
45 Draix–Bléone catchments, but improved identification and understanding of the weathering processes in these marls are  
required to more accurately predict exported sediment volumes.

Several studies have addressed the characteristics and dynamics of regolith development in the marly badlands of the Draix-  
Bléone CZO and similar sites. The impact of water content, hydraulic conductivity and infiltration capacity of marls in the  
Draix-Bléone CZO on runoff generation and erosion was studied by Esteves et al. (2005), Mathys et al. (2005) and Mallet et  
50 al (2018). Rovéra and Robert (2005) first investigated periglacial erosion processes in the Draix-Bléone CZO; they noted the  
marls’ sensitivity to frost weathering and the distinct evolution of the regolith between south-facing and north-facing slopes.  
Working in the Central and Eastern Spanish Pyrenees, Regüés et al. (1995) and Nadal-Romero et al. (2007) confirmed the  
important role of slope aspect in controlling the weathering of marls. By studying bulk density, surface mechanical resistance  
and moisture content, they highlighted a clear temporal and spatial variability in the regolith and inferred that weathering in  
55 these catchments was mainly dependent on the number of freeze-thaw cycles occurring during the year. Based on a time series  
of high-resolution digital elevation models from a 0.13 ha catchment in the Draix-Bléone CZO, Bechet et al (2016) showed  
that erosion processes follow a seasonal cycle, with accumulation of loose regolith on slopes during winter followed by its  
transport from the slopes to the main gullies during summer. These authors inferred a yearly cycle between transport-limited  
conditions in spring to supply-limited conditions in autumn. However, Jantzi et al. (2017) used sediment-budget calculations  
60 from the larger Moulin and Laval catchments of the Draix-Bléone CZO (see below) to infer that sediment transfer is not  
immediate; they calculated a 3-year residence time for sediments in these catchments.



Overall, existing observations from the Draix-Bléone CZO and similar sites lead to consider frost -weathering as a potentially important process controlling regolith production in marly Alpine badlands. Several studies have explored this process in different geological contexts, employing theoretical, experimental and observational approaches. The two main frost-  
65 weathering processes considered in the literature are volumetric expansion of ice and ice segregation (e.g., Matsuoka, 2008). Volumetric expansion of ice can occur repeatedly during freeze-thaw cycles, whereas ice segregation occurs when liquid water migrates towards a locus of ice-lense growth. In cold and high Alpine environments, it appears that ice segregation controls rock weathering by widening rock fractures or “frost cracking” (Anderson, 1998; Matsuoka and Murton, 2008). The growth  
70 of ice lenses required for frost cracking has been argued to depend primarily on absolute temperature, water availability and temperature gradient (Hallet et al., 1991). Hales and Roering (2007) developed a numerical model to estimate soil temperature at different depths and defined a frost-cracking intensity indicator to quantify ice-driven mechanical erosion. In their model, frost cracking occurs when rocks are in the “frost-cracking window” (between -3 and -8 °C) and liquid water is available because either the surface or rocks at depth are above freezing point; the frost-cracking intensity depends on the temperature  
75 gradient in the frost-cracking window. Subsequently, Anderson et al. (2013) modelled rock damage by frost cracking using the above model, adding the distance that water must travel to reach the locus of potential frost cracking, and observed the impact on regolith production and hillslope evolution.

The above models have, however, not yet been applied in more temperate/humid climates and in soft lithologies. Two previous studies invoking frost weathering in these contexts (Rovéra and Robert, 2005; Nadal-Romero et al., 2007) only addressed the number of freeze-thaw cycles, and thus implicitly frost weathering by volumetric expansion. Additionally, the link between  
80 regolith production and sediment yield is known but remains difficult to quantify. Rengers et al. (2020) recently bridged this gap by studying plot-scale (22 m<sup>2</sup>) sediment accumulation and debris-flow channel filling patterns using repeat topographic surveys. They found a strong correlation between frost-cracking intensity and sediment production in a steep Alpine bedrock setting.

In this study, we develop a similar approach at the catchment scale (0.1-1 km<sup>2</sup>) in marly badlands. At this scale, sediment  
85 export is primarily driven by rainfall, particularly during high-intensity events (Mathys et al., 2003), but we hypothesize that frost-weathering processes can modulate sediment yield by controlling regolith production on hillslopes. To test our hypothesis, we used high-resolution soil-temperature measurements from different locations and compared calculated temperature indicators, including the number of freeze-thaw cycles, the time spent below 0 °C, the mean negative temperature and the frost-cracking intensity, during a winter season to the sediment-export anomaly (i.e., the residual of sediment yield  
90 that cannot be explained by rainfall variability) in the following year. The goal of our study is threefold: (1) to confirm the seasonal variability of regolith supply by analysing monthly total sediment yield; (2) to quantify the role of frost-weathering processes in yearly sediment production; and (3) to identify the relevant weathering processes by statistical analysis of different proxy indicators.



## 2. Study site

95 The Draix-Bléone CZO is part of the French network for the study of the critical zone OZCAR (Gaillardet et al., 2018) and is specifically dedicated to the study of erosion and sediment transport in a mountainous region. Hydrological and sedimentary fluxes have been monitored on several catchments in this CZO since 1983 (Draix-Bléone Observatory, 2015). The Draix-Bléone CZO is situated in the Alpine foothills, 12 km northeast of the town of Digne in South-East France (Fig. 1). The Draix catchments are drained by the Bouinenc stream, a tributary of the Bléone, which is itself one of the main tributaries of the  
100 Durance River. The geology is characterised by Mesozoic sediments that were folded and faulted during the Alpine orogeny (Lemoine et al., 1986; Lickorish and Ford, 1998). The Bouinenc catchment has a mountainous and Mediterranean climate. Due to its relatively high elevation (>800 m above sea level), the mountainous influence is responsible for cold winters with frequent frost. The Mediterranean influence leads to dry summers interspersed by intense thunderstorms. Annual rainfall is about 900 mm/yr (varying between ~600 and ~1300 mm/yr interannually) in Draix. The rainfall regime varies across seasons,  
105 with high-intensity rainfall events during spring/summer and lower-intensity but longer rainfall events in autumn. The mean annual temperature is 10.3 °C, with an annual variability between mean daily temperatures of approximately 0.5 °C in winter and 20 °C in summer.

This study focuses on two instrumented catchments of the Draix-Bléone CZO: the Laval and the Moulin catchments, which have drainage areas of 0.86 and 0.10 km<sup>2</sup>, respectively. Elevations vary between 850 and 1250 m in these catchments.  
110 Vegetation cover is 46% in the Moulin and 32% in the Laval catchment (Carriere et al., 2020). The catchments are underlain by thick Middle-Jurassic black marl series locally known as “Terres Noires”. Subtle changes in composition of the marls, with a limestone fraction varying according to stratigraphic level, have been observed (Brochot, 1997) but our study site is not affected by these variations. The dominant bedding dip is to the east in the Draix area. These black marls are susceptible to strong erosion and develop steep badland slopes (Fig. 1C, D) with high drainage density and deeply incised gullies  
115 characterizing the catchment morphologies. The Draix catchments records some of the highest observed specific sediment yields worldwide: average annual sediment yields are around 12,000 and 570 tonnes for the Laval and Moulin catchments, respectively. Considering only the unvegetated parts of the catchments as contributing to the sediment yield, the average erosion rate is around 8 mm/yr (Mathys, 2006).

## 3. Methods

### 120 3.1 Data acquisition

We use three types of datasets: rainfall, sediment yield and soil temperature. Monthly and annual rainfall values are obtained by summing the detailed event records measured with a tipping-bucket rain gauge located at the outlet of the Laval catchment (Fig. 1C). Sediment yield is measured at the outlets of both the Laval and Moulin catchments, where hydro-sedimentary



stations have been set up to monitor water discharge and both suspended load and bedload. Suspended sediment concentration  
125 is measured with automatic samplers and turbidimeters and suspended sediment flux is computed as the product of discharge  
and concentration, cumulated over a flood to obtain an event-scale yield. Bedload volumes are measured after each flood by  
topographic surveys of a sediment trap located upstream of the station. Bedload volume is then converted into mass using a  
density of  $1700 \text{ kg/m}^3$ , constrained by measurements in the sediment trap (Mathys, 2006). Thus, the raw data correspond to  
event-scale values and the total sediment export used in this study refers to the monthly or yearly sum of the suspended load  
130 and bedload contributions. For a few flood events, the suspended-load data is missing. In such cases, we reconstructed the  
event-scale suspended sediment yield based on the average proportions of suspended load and bedload, computed from  
multiple complete years of total load records. The proportions of suspended load and bedload in the Laval catchment are 74%  
/ 26% for summer floods (May to September) and 57% / 43% for winter floods (October to April).

Soil temperature has been recorded using several PT100 soil-temperature probes located on opposite slopes in an inner meander  
135 of the Moulin Creek between August 2005 and December 2019 (Fig. 1C, D). The acquisition frequency was 10 minutes. We  
use the data from probes located in bare black marls at uphill and downhill locations on north- and south-facing slopes,  
respectively (Fig. 1D), in order to explore variations in soil temperature due to differences in exposure (Rovéra and Robert,  
2005). At each location, four probes are available to measure soil temperature at depths of 1, 6, 12 and 24 cm, respectively.  
As our interest is focused on frost weathering, we specifically analysed soil temperatures during the winter season, from  
140 October 18<sup>th</sup> to March 31<sup>st</sup>. This period was chosen because (1) negative soil temperatures are almost absent outside these  
dates; (2) some series miss temperature data for early October.

The soil-temperature dataset includes periods of missing or spurious data, due to probe malfunction, unearthing or burial. The  
relatively mobile nature of the marls leads to frequent displacement of probes, identified in the temperature records by similar  
temperatures between probes at different depths or anomalous daily temperature ranges (Fig. 2). When these periods are longer  
145 than fifteen consecutive days, the full season of data is rejected (i.e., 2005/2006, 2010/2011 and 2012/2013). When the missing  
period is shorter (for seasons 2011/2012 and 2014/2015), we searched for a relation between soil temperature and air  
temperature (recorded at the closest weather station) in order to reconstruct soil temperature during the missing time interval.  
We found that a simple two-tier linear fit predicted soil temperature well for air temperature below  $10 \text{ }^\circ\text{C}$  and soil temperature  
below  $5 \text{ }^\circ\text{C}$ , with an inflexion point around  $-4 \text{ }^\circ\text{C}$ . The correlation breaks down for higher temperatures due to radiative heating  
150 effects; however, since our focus is on soil temperatures below  $0 \text{ }^\circ\text{C}$ , the simple linear-correlation approach is sufficient. The  
presence of snow sets the soil temperature to  $\sim 0 \text{ }^\circ\text{C}$  (Fig. 2) and thus perturbs the linear trend. Therefore, the regression was  
calibrated during snow-free periods only.



## 3.2 Data Processing

### 3.2.1 Rainfall and sediment export

155 As established in previous studies (Mathys et al., 2003; Bechet et al., 2016), sediment export at the event scale is driven by  
rainfall intensity above a threshold. Therefore, we analysed the correlation between annual sediment export and annual rainfall,  
looking not only at total annual rainfall, but also at annual rainfall above several threshold values varying from 10 to 80 mm/h.  
We selected this range of thresholds based on inferences from previous studies and then used the value providing the best  
correlation to predict annual sediment-export values. In order to stay in phase with the period where soil temperature data were  
160 available, we used only data between 2005 and 2019 for the correlation between rainfall and annual sediment export. We  
defined the sediment-export anomaly as the residual between measured sediment export in any year and the predicted value  
from this regression. Here, we aim to identify a controlling factor to explain this sediment-export anomaly.

### 3.2.2 Temperature indicators

With the aim of identifying the impact of frost weathering on sediment production, we selected four potential indicators of  
165 frost-weathering intensity and correlated them both with each other and with the sediment-export anomaly.

First, we computed the Frost Cracking Intensity Indicator (FCII) based on the model of Hales and Roering (2007), inspired by  
the segregation ice-growth hypothesis of Hallet et al. (1991). Because reliable data on soil moisture are very challenging to  
obtain in marly badlands, we considered, based on the work by Mallet et al. (2018), that the marls fulfil the moisture conditions  
needed for ice-lens growth during winter. Since we had access to direct soil-temperature measurements at different depths, we  
170 used these rather than the diffusive model based on air-temperature developed to predict soil temperatures in the original  
formulation of Hales and Roering (2007). The soil-temperature gradient was computed between the probes located at 1 cm  
and 24 cm depth. We summed temperature gradients during all time intervals when the surface temperature (probe at 1-cm  
depth) was within the frost-cracking window (between -3 and -8 °C) over a winter cycle, and used this number as a proxy for  
the frost-cracking intensity. Following Anderson et al. (2013), we expressed the FCII in units of temperature-time/length (°C  
175 min/cm in our case). The probes at 24 cm depth on the north-facing slope did not produce reliable data for almost all years  
considered; we therefore only computed FCII for the south-facing slope.

The second indicator counts the number of freeze/thaw cycles as a proxy for the efficiency of frost weathering by volume  
expansion. The raw temperature data include many insignificant temperature fluctuations around 0 °C, over very short periods  
that do not allow the formation of frost. We therefore applied a time threshold of 1 hour below 0 °C to count a freeze/thaw  
180 cycle. The same duration was considered as a threshold for temperature remaining above 0 °C to distinguish two freezing  
periods. We observed that increasing this threshold to more than 1 hour did not affect the number of freeze/thaw cycles  
significantly; above this threshold the number of cycles tended toward counting the daily temperature cycles.



185 The third indicator is the time spent at negative temperatures. We counted the number of 10-minute periods with negative temperature recordings at the 1 cm-depth probe and converted these into hours. Finally, the fourth indicator is the mean negative temperature, which was computed as the mean temperature value when it is below zero, again for the 1 cm-depth probe. The behaviours of these indicators were found to be very different between south-facing and north-facing sites, whereas they did not vary much between uphill and downhill sites. Therefore, we analysed them by averaging the value of the uphill and downhill indicators for each slope aspect.

### 190 3.2.3. Uncertainties

We accounted for uncertainty in our analyses using the following procedures. We defined the uncertainty on the sediment-export anomaly resulting from the linear regression between rainfall and sediment export as the 2- $\sigma$  error on the sediment-export values predicted by the regression. Whereas the sediment-export and rainfall measurements are associated with uncertainties themselves, these are insignificant with respect to the uncertainty on the regression and were therefore not included in the analysis. For the temperature indicators, we defined the uncertainty around their mean value by the difference between the value of the indicator obtained at the uphill and downhill location on the same slope (i.e., north-facing versus south-facing).

To establish a relation between sediment-export anomalies and temperature indicators while accounting for these uncertainties in both parameters, we used weighted linear regression with the uncertainty in both independent and dependent variables as (inverse) weights (cf. York et al., 2004). Since a conventional  $R^2$  is invalid in the presence of measurement errors (Cheng et al., 2014), we characterise the quality of the weighted regressions by a weighted correlation coefficient  $R^2_w$  computed from the weighted residual ( $\text{Var}_{\text{res-w}}$ ) and weighted total ( $\text{Var}_{\text{tot-w}}$ ) variance ( $R^2_w = 1 - (\text{Var}_{\text{res-w}} / \text{Var}_{\text{tot-w}})$ ). The goodness-of-fit of the weighted correlation is expressed by the weighted sum of deviations from the best-fit line  $S$ , normalised by the degrees of freedom ( $n-2$ ):  $S_n = S / (n-2)$  (York et al., 2004). We also computed standard  $R^2$  and p-values from an ordinary least-squares linear regression as these are more readily interpreted in terms of significance of the regression. Because of the apparent differences in correlations between the north-facing and south-facing slopes, we analysed correlations for both slope aspects separately.

## 4. Results

### 4.1. Seasonal variability in sediment export

210 Box plots of monthly precipitation and total sediment export (i.e., bedload and suspended load) recorded between 2003 and 2019 show high disparity between monthly averages and significant interannual variation for each month (Fig. 3). Median monthly rainfall values vary from  $\sim 50$  mm in January-March to  $\sim 100$  mm in October-November, with extreme values reaching



~300 mm in those months. The variability in monthly total sediment export is higher, with minimum and maximum values of median sediment export around 0 and 3.6 ktons in March and June, respectively. Extreme values reach almost 10 ktons.

215 For both sediment export and rainfall, higher monthly values are associated with higher variability (i.e., values for June and November, respectively). Most months show outlier values and distributions of total sediment export are skewed toward high values (mean > median). Rainfall boxplots show a larger spread between the first and third percentiles but more symmetric distributions.

Despite noticeable disparities between years (Figs. 3B, 4A), mean values highlight a strong seasonal pattern in precipitation and sediment export, as previously observed (Mathys et al., 2003; Fig 4B). In the Laval catchment, sediment export is low in winter and increases in spring to a peak in June, with an average monthly export of >3.4 ktons, despite relatively low total rainfall during that month (<80 mm). Conversely, autumn months (October, November) are characterized by high total rainfall (>100 mm/month) but much lower sediment export (<2 ktons/month). Despite their difference in size, the monthly distribution of total sediment export is similar between the Moulin and Laval catchments (Fig. 5): both show a major peak in June, amounting to ~20% of total yearly sediment export, with smaller peaks (~10%) in August and October. The monthly rainfall distribution shows a main peak in October-November, with a secondary peak in May. The spring rainfall peak (May) occurs one month earlier than the sediment-export peak (June) for both catchments.

220  
225

Based on annual data records since 2005 and previous work (see Methods section), we established a correlation between rainfall intensity above a threshold and sediment export (Fig. 6). An optimal correlation is obtained for a threshold of 50 mm/h ( $R^2 = 0.88$ ), with most scatter occurring for cumulative rainfall (above threshold) values between 0 and 40 mm. This correlation was used to define the sediment-export anomaly as the residual between observed and predicted annual sediment-export values for each year.

230

### 4.3. Potential temperature control on sediment export

235 Daily temperature fluctuations in the bare marly soils that were monitored are significantly higher for the shallow (-1 cm) than for the deep (-24 cm) sensors (Fig. 2). During summer, surface temperatures show a daily variability of ~40 °C (between ~10 °C at night and ~60 °C at midday), whereas the daily variability in winter averages around 20 to 30 °C depending on aspect. These daily variabilities decrease drastically with depth, fluctuating generally within 5 °C and 20 °C for the probes at -24 cm and -12 cm depth respectively, but can occasionally be higher. The maximum daily temperature is reached asynchronously according to the exposure; in the north-facing hillslope, maximum temperature occurs in the morning (around 10 am), whereas in the south-facing slope it occurs late in the afternoon (around 4 pm). At the maximum depth (-24 cm), minimum soil temperatures during winter are negative on the north-facing slope but positive on the south-facing slope.

240

We calculated four different temperature indicators during the winter months, as explained in section 3.2.2, and compared these with each other as well as with the sediment-export anomaly obtained previously, in order to (1) assess the degree of co-



245 variation between the different indicators, and (2) characterize the direction and strength of the relationship between the  
temperature indicators and the sediment-export anomaly. Overall, stronger correlations were found between temperature  
indicators on the south-facing slope than on the north-facing slope (Fig. 7). Frost-cracking intensity, which was only computed  
on the south-facing slope, correlates strongly ( $|R| > 0.7$ ) with the other temperature indicators. Time below  $0\text{ }^{\circ}\text{C}$  is also strongly  
correlated with the number of freeze-thaw cycles / year ( $R = 0.85$ ) on the south-facing slope. All of the correlations between  
250 temperature indicators are significant ( $p < 0,05$ ) on the south-facing slope. On the north-facing slope, in contrast, the only  
significant correlation between temperature indicators occurs between the number of freeze-thaw cycles / year and mean  
negative temperature ( $R = -0.62$ ). Sediment-export anomalies correlate most strongly with frost-cracking intensity on the  
south-facing slopes ( $R = 0.80$ ) but are also significantly correlated with time below  $0\text{ }^{\circ}\text{C}$  ( $R = 0.71$ ). On the north-facing slope,  
the only significant correlation occurs between sediment-export anomaly and time below  $0\text{ }^{\circ}\text{C}$  ( $R = 0.74$ ), but note that frost-  
255 cracking intensity was not calculated on the north-facing slope.

These correlation results led us to investigate how much of the variability in sediment-export anomalies can be explained by  
these different temperature indicators, taking in account the uncertainties on both measures (Figs. 8, 9). Results show that the  
weighted regression between frost-cracking intensity and sediment-export anomalies can explain 47% of the variance in the  
latter ( $R_w^2 = 0.47$ ). The ordinary least-squares (OLS; i.e., unweighted) correlation is significant ( $p = 0.03$ ) and only slightly  
260 deviates from the weighted regression (Fig. 8). Based on this trend, the highest sediment-export anomalies appear to occur in  
years succeeding winters with strong (negative) frost-cracking intensity.

A significant positive relationship is also found between sediment-export anomalies and time below  $0\text{ }^{\circ}\text{C}$  on both the south-  
facing ( $R_w^2 = 0.69$ ) and north-facing ( $R_w^2 = 0.40$ ) slopes (Fig. 9). In contrast, regressions between sediment-export anomalies  
and either the number of freeze-thaw cycles / year or the mean negative temperature are not significant on either slope and  
265 show an opposite trend between slopes (i.e., a positive correlation on one slope and negative on the other; Fig. 9). This analysis  
suggests that both the frost-cracking intensity (where it can be calculated) and the time spent below  $0\text{ }^{\circ}\text{C}$  in a particular winter  
are good predictors of sediment-export anomalies (deviations from sediment export predicted by rainfall over a threshold) in  
the following year.

## 5. Discussion

### 270 5.1. Limitations of our study

Because of the strong annual and interannual variability in regolith cover and sediment export, long-term field measurements  
at high spatial and temporal resolution are required to characterise the dynamics of badland erosion. The Draix-Bléone CZO  
provides one of the few localities worldwide where such records exist. However, uncertainties in both sediment-yield records  
and soil-temperature measurements are inevitable and difficult to estimate.



275 The interpretation of the hysteresis cycle (Fig. 4) should integrate the variability in sediment export (Fig. 3). Although June  
shows the highest sediment export overall, this month is also characterised by the highest inter-annual variability in sediment  
export. This variability can be explained by the stochastic nature of precipitation, which occurs mainly due to storms during  
the spring and summer seasons. Thus, sediment-export values for June vary between 0 (no large rainfall events during the  
month) up to 8000 tons. The monthly data show that the highest sediment export can also occur in July (and more rarely in  
280 August) in some years. In order to smooth out such stochastic behaviour, we integrated sediment-export values over the full  
year following each investigated winter season.

The export-anomaly values that we computed are dependent on the linear regression with rainfall above a threshold (Section  
4.1; Fig. 6). Extreme values, such as the three years with  $>70$  mm or more rainfall above the 50 mm/h threshold, have an  
important impact on the regression and thus on the export-anomaly values. Calculating uncertainties on the annual sediment  
285 export is challenging, but an order of magnitude of around 10% of the total sediment export can be estimated. This uncertainty  
is negligible compared to the uncertainties on sediment-export anomalies that we infer from the regression analysis. The  
uncertainty on annual rainfall is also considered negligible.

Soil-temperature probes have proven very difficult to maintain at the depths where they were installed in the soft, mobile marls  
of our study area. For this reason, we could only calculate frost-cracking intensity (which requires concomitant data from the  
290 -1 cm- and -24 cm-depth probes) for the south-facing slope and for only 7 years between 2005 and 2019 (Fig. 8). We therefore  
searched for a temperature proxy that allows predicting frost-weathering intensity with less constraints on the data, and found  
that the time spent below 0 °C (for the -1 cm-depth probe) can be a useful indicator.

When assessing the predictive power of the different temperature indicators to explain sediment-export anomalies, we aimed  
to take into account the uncertainties in both variables (Figs. 8, 9) by employing weighted regression based on uncertainties  
295 (York et al., 2004). However, the uncertainties in temperature indicator values were computed from only two points, i.e., the  
measurements at the uphill and downhill locations of each slope aspect. Uncertainties on both variables should also be of the  
same order of magnitude to avoid biasing the weighted regression, whereas in our case, the relative uncertainties in the  
temperature indicators can be much larger than those in the sediment-export anomalies. For this reason, we also report the  
ordinary least-squares regression and associated significance (p-value).

300

## 5.2. Significance of the observed hysteresis cycle

Numerous studies have reported annual hysteresis cycles between rainfall or discharge on one hand, and sediment export on  
the other; these studies, have commonly focused on large catchments, e.g. in the Andes or Himalaya (e.g., Andermann et al.,  
2012; Armijos et al., 2013; Tolorza et al., 2014; Li et al., 2021). For such large catchments, the annual hysteresis cycle is  
305 explained by the role of subsurface water storage (Andermann et al., 2012), dilution effects (Armijos et al., 2013) or variations  
in the contributive erosive area (Li et al., 2021). Hysteresis cycles for smaller catchments have generally been analyzed at the



event scale, and have been interpreted in terms of the proximity of sediment sources and the spatio-temporal heterogeneity of rainfall (e.g., Klein, 1984; Buendia et al., 2016). In a catchment of intermediate size (440km<sup>2</sup>), Buendia et al. (2016) also highlighted a seasonal lag between discharge and sediment yield response, which they related to transient in-channel storage.

310 The annual hysteresis cycle between rainfall and sediment export observed in the Draix-Bléone CZO (Fig. 4) presents two loops with successively anti-clockwise and clockwise patterns, reflecting the rapid seasonal changes in erosion regime in these badlands. We interpret the initial anti-clockwise hysteresis loop, with sediment export lagging behind precipitation in the first half of the year, to be due to the threshold in rainfall intensity required to generate erosion; although rainfall is high in spring, it is also of low to moderate intensity. It is only with the high-intensity storms of late spring/early summer that significant

315 amounts of sediment are exported from the catchment. The initial anti-clockwise hysteresis loop thus indicates transport-limited conditions. In contrast, the clockwise loop characterising the second half of the year indicates supply-limited conditions, with the supply of mobile sediments running out after summer (Bechet et al., 2016). A similar trend appears in the Moulin catchment, despite its much smaller catchment area (Fig. 5). This seasonal pattern does not seem to change with recent climatic variations because it was already reported by Mathys et al. (2003), who analysed the seasonality of bedload yield

320 based on Draix-Bléone observatory data between 1985 and 2003.

The annual pattern that we describe in Fig. 4 characterizes the total sediment export, which is the sum of the suspended sediment and bedload yield. According to the observations of Mathys et al. (2006) and Liébault (2017), highest export values for bedload occur during autumn. However, this trend is modified when adding the suspended load because the exported suspended-sediment mass can be up to four times higher than bedload-sediment mass during spring. A similar ratio has been

325 observed in other catchments (Lana-Renault and Regüés, 2007; Rainato et al., 2017) and leads to the present result where late spring/early summer (more specifically, June) is the period that contributes most to the total sediment yield. Thus, sediment dynamics vary according to grain size: intense precipitation events during late spring/early summer mobilise the regolith produced during the winter, and suspended sediments are transported almost directly from the hillslopes to the catchment outlet. In contrast, coarser bedload sediments are deposited in gullies during these short intense events and are only exported

330 by the lower-intensity but longer-duration rainfall events of the autumn. These dynamics suggest that suspended sediment storage is almost non-existent in the Moulin and Laval catchments, whereas bedload sediment can be stored for several months.

### 5.3. Frost weathering as a major control on sediment production in the Draix-Bléone CZO

The significant correlations between frost-cracking intensity or time below 0 °C and sediment-export anomalies imply that frost-weathering processes constitute a major secondary control on sediment export. While the main control on the yearly

335 amount of sediment exported from the studied catchments is exerted by rainfall above a threshold (Fig. 6), the efficiency of frost-weathering processes during the preceding winter, as expressed by the frost-cracking intensity indicator or the time below 0 °C, can explain about half of the residual from this trend (Figs. 8, 9). Together with the evidence for a transition from transport-limited to supply-limited conditions during the year discussed above, we interpret these results as indicating that



340 frost-weathering processes modulate sediment export from the catchments by exerting a strong control on the production of mobilizable sediment. These findings are consistent with those of Rengers et al. (2020), who found a strong positive correlation between the time spent in the frost-cracking window and sediment production feeding debris-flow channels on a small, steep plot in the Rocky Mountains of Colorado. The similar results between both studies, despite differing scales, lithologies and geomorphic settings, attest to the potential widespread control of frost-weathering processes on sediment production.

345 Additionally, our results like those of Rengers et al. (2020) show a weak correlation between sediment production and the number of freeze-thaw cycles per year. As discussed in the introduction, freeze-thaw cycles are associated with volumetric expansion of ice, whereas frost-cracking is related to ice segregation. Thus, the migration of liquid water to loci of ice-lense growth appears to be a more efficient process of soil weathering than volumetric expansion, even in this temperate and moderate-elevation environment. Nadal-Romero et al. (2007) similarly concluded that frost-weathering processes play an important role in weathering of marly badlands in northern Spain; they also demonstrated significant variations between north-  
350 facing versus south-facing slopes. However, Nadal-Romero et al. (2007) focused their attention on freeze-thaw cycles and did not investigate frost-cracking, the quantification of which requires more data. Nonetheless, our studies concur in underlining the influence of frost-weathering processes on regolith development as well as important spatial variations between north- and south-facing slopes, supporting the theoretical predictions of Anderson et al. (2013).

355 Directly quantifying frost-cracking intensity (rather than inferring it from atmospheric temperature data) requires dense and high-quality field data, in particular concomitant soil-temperature data at multiple depths to quantify thermal gradients. Even in permanently monitored long-term observatories such as Draix-Bléone, such data may be rare. However, our study suggests that the time spent below 0°C may be used as a simpler proxy to predict frost-weathering intensity. Our weighted regressions show that this indicator correlates well with the sediment export anomaly and captures the effect of frost-weathering processes on sediment production, even though uncertainties in the regression can be significant (in particular on the south-facing slope  
360 in our case). In contrast, neither the mean negative temperature nor the number of freeze-thaw cycles appear as reliable proxies to estimate frost weathering in this setting.

365 These correlations between sediment production computed during a winter season and sediment yield for the directly following year (spring to autumn), together with the strongly varying dynamics of transport during the year discussed in the previous section, favour the hypothesis of rapid sediment export from the studied catchments, in contrast to the 3-year residence time of sediments in these catchments inferred by Jantzi et al. (2017). In order to test this hypothesis, we performed correlations between the frost-cracking intensity in a particular winter season and the sediment-export anomaly of the first, second and third year after that season (i.e., in the last case, if we consider the 2006-2007 winter season for the frost-cracking intensity, we compare it to the sediment-export anomaly for 2010). In all configurations, the correlation is weaker than the direct annual correlation that we observed ( $r = 0.80$ ); in particular, the  $n+3$  correlation shows  $r = -0.53$  and is not significant ( $p = 0.076$ ).  
370 The ratio observed in sediment distribution during the spring/summer (74% suspended load / 26% bedload) and the rapid export of these fine sediments probably make the suspended load invisible in the estimation of sediment storage in the catchment, rendering the calculation of residence time complex. Thus, it appears that the Laval catchment has an efficient



drainage system, with high connectivity and low sediment storage, which does not contribute significantly to the production /  
export balance. Similar short residence times have been observed, at a different scale, in a similar environment in northern  
375 Spain (Andres Lopez-Tarazon et al., 2011).

#### 5.4. Implications for the erosional response to climate change

Due to their limited vegetation cover and soft lithology, badlands are sensitive areas that are directly exposed to climatic  
parameters and thus will respond quickly to even small climatic variations. In the context of anthropogenic climate change,  
weathering or erosion processes and hydrology will necessarily be modified: a positive or negative variation of one of these  
380 main operating processes could be balanced against others but could also be additive, thereby inducing important changes in  
morphology and sediment export in these landscapes.

Based on a review of multiple badland areas in the Mediterranean region, Nadal-Romero et al. (2021) have recently  
investigated the impact of climate change on these particular landscapes, taking into account different climate-drivers (rainfall  
amount, rainfall intensity, wetting-drying cycles, freeze-thaw cycles, soil moisture content, etc.). Their analysis predicts that  
385 for wet badlands such as Draix-Bleone, the expected increase in rainfall intensity should increase erosion capacity on one  
hand, but that the expected increase in temperature should lower the number of freeze-thaw cycles, thereby reducing the  
efficacy of frost-weathering processes and decreasing sediment availability on the other hand. Considering the result from our  
study that frost-cracking intensity, and not freeze-thaw cycles, is the best indicator for sediment production by frost-weathering  
processes, the frost intensity rather than the number of frost days should present a better proxy to predict the evolution of  
390 sediment availability. However, the time spent below 0°C, identified here as a simple alternative proxy for frost-weathering  
intensity, will also be directly affected by an increase in temperature and similarly lead to a decrease in sediment production  
in a warming climate.

Recently, Hirschberg et al. (2021) have also shown that projected changes in precipitation and air temperature would lead to  
a reduction in both sediment yield and debris-flow activity in an Alpine catchment at moderate elevation (< 2000 m), because  
395 of the reduction of frost-weathering intensity. In general, expected changes in sediment production in temperate regions under  
a warming climate appear to have a counter-effect to the predicted increase in average rainfall amounts and intensities, which  
have been considered as “the most direct factors controlling erosional changes under climate changes” (Nearing et al., 2004).  
This complex interaction between sediment production and sediment transport underlines the necessity to account for the  
processes responsible for sediment production in longer-term predictions of sediment yield.

400 Finally, in addition to physical weathering processes that are discussed here, chemical and biological weathering processes  
also play an important role in rock-weathering and will also be affected by precipitation and temperature changes (West et al.,  
2005, Brantley et al, 2011). Additionally, erosion processes could be impacted by changes in the vegetation but this interactions  
are particularly complex to understand (Nearing et al., 2004). Therefore, climatic variations may change the balance between



405 weathering and erosional processes as well as their timing, leading to complex positive or negative feedbacks on catchment erosion that remain difficult to predict.

## 6. Conclusions

Based on our analysis of sediment-yield records and soil-temperature data from the Draix-Bléone CZO and accounting for the inevitable uncertainties in our dataset, we show that frost-weathering processes modulate sediment export by controlling sediment production in these marly catchments. Our main conclusions are summarized below:

- 410 • Monthly total sediment export (suspended load and bedload) is highly variable and shows a seasonal pattern. The annual hysteresis cycle (Fig. 4) shows an anti-clockwise pattern during spring and a clockwise pattern later in the year, suggesting an initial transport-limited regime followed by a supply-limited regime in these catchments.
- Total annual sediment export is well correlated with rainfall above an intensity threshold; a threshold of 50 mm/h maximises the correlation (Fig. 6).
- 415 • The frost-cracking intensity indicator, calculated following the Hales and Roering (2007) model, explains about half of the sediment-export anomaly (Fig. 7), implying that the process of frost weathering through ice segregation strongly controls regolith production and modulates sediment export.
- The time spent below 0°C is an easier to measure and simpler proxy, and is also an indicator of frost-weathering intensity that correlates well with the sediment export anomaly (Fig. 7). In contrast, neither the number of freeze-thaw cycles nor  
420 the average negative temperature during a winter season show significant correlations with sediment-export anomalies.
- South- and north-facing slopes show distinct behaviour with respect to frost-weathering processes, confirming observations from previous studies.
- Frost-weathering processes should be taken into account when building predictive models of sediment export under a changing climate. Under a warming climate, frost weathering should become less important, counteracting the increased  
425 sediment export expected from a stormier climate.

The long-term monitoring records available for the Draix-Bléone CZO catchments have allowed identifying frost-cracking by ice segregation as a major control on sediment production. Further assessment of the importance of this process would require similar studies in different environments (e.g., drier climates, more vegetated areas, higher elevation, etc.) and at different catchments scales. Field measurements of sediment export and soil-temperature are on-going in the Draix-Bléone observatory  
430 and additional data could be incorporated to the present results in the next few years. In a context of global climate change, future measurements might illustrate the consequences of climate variations at human timescales on processes in the critical zone.



## Data Availability

The sediment yield data used in this manuscript is available on BDOH data portal: <https://bdoh.irstea.fr/DRAIX/> and  
435 referenced under the dynamic identifier doi:10.17180/OBS.DRAIX.

## Acknowledgements

This research has been supported by the French National Research Agency (ANR) under the grant ANR-18-CE01-0019-01 (DEAR project) and INRAE Grenoble. This study was carried out in the Draix-Bléone Observatory (France) and used its infrastructure and data. The Draix-Bléone Observatory is funded by INRAE (National Research Institute for Agriculture, Food  
440 and Environment), INSU (National Institute of Sciences of the Universe) and OSUG (Grenoble Observatory of Sciences of the Universe) and is part of the French network of Critical Zone Observatories OZCAR, which is supported by the French Ministry of Research, French Research Institutions and Universities.

## References

- 445 Andermann, C., Bonnet, S., Crave, A., Davy, P., Longuevergne, L., and Gloaguen, R.: Sediment transfer and the hydrological cycle of Himalayan rivers in Nepal, *C.R. Géosci.*, 344, 627–635, <https://doi.org/10.1016/j.crte.2012.10.009>, 2012.
- Anderson, R. S.: Near-surface thermal profiles in alpine bedrock: Implications for the frost weathering of rock, *Arct. Alp. Res.*, 30, 362–372, 1998.
- Anderson, R. S., Anderson, S. P., and Tucker, G. E.: Rock damage and regolith transport by frost: an example of climate modulation of the geomorphology of the critical zone: *Earth Surf. Process. Landf.*, 38, 299–316,  
450 <https://doi.org/10.1002/esp.3330>, 2013.
- Anderson, S. P., Anderson, R. S., and Tucker, G. E.: Landscape scale linkages in critical zone evolution, *C.R. Géosci.*, 344, 586–596, <https://doi.org/10.1016/j.crte.2012.10.008>, 2012.
- Andres Lopez-Tarazon, J., Batalla, R. J., and Vericat, D.: In-channel sediment storage in a highly erodible catchment: the River Isabena (Ebro Basin, Southern Pyrenees), *Z. Geomorphol.*, 55, 365–382, <https://doi.org/10.1127/0372-8854/2011/0045>,  
455 2011.
- Antoine, P., Giraud, A., Meunier, M., and Van Asch, T.: Geological and geotechnical properties of the “Terres Noires” in southeastern France: Weathering, erosion, solid transport and instability, *Eng. Geol.*, 40, 223–234, [https://doi.org/10.1016/0013-7952\(95\)00053-4](https://doi.org/10.1016/0013-7952(95)00053-4), 1995.
- Armijos, E., Crave, A., Vauchel, P., Fraizy, P., Santini, W., Moquet, J.-S., Arevalo, N., Carranza, J., and Guyot, J.-L.:  
460 Suspended sediment dynamics in the Amazon River of Peru, *J. S. Am. Earth Sci.*, 44, 75–84, <https://doi.org/10.1016/j.jsames.2012.09.002>, 2013.



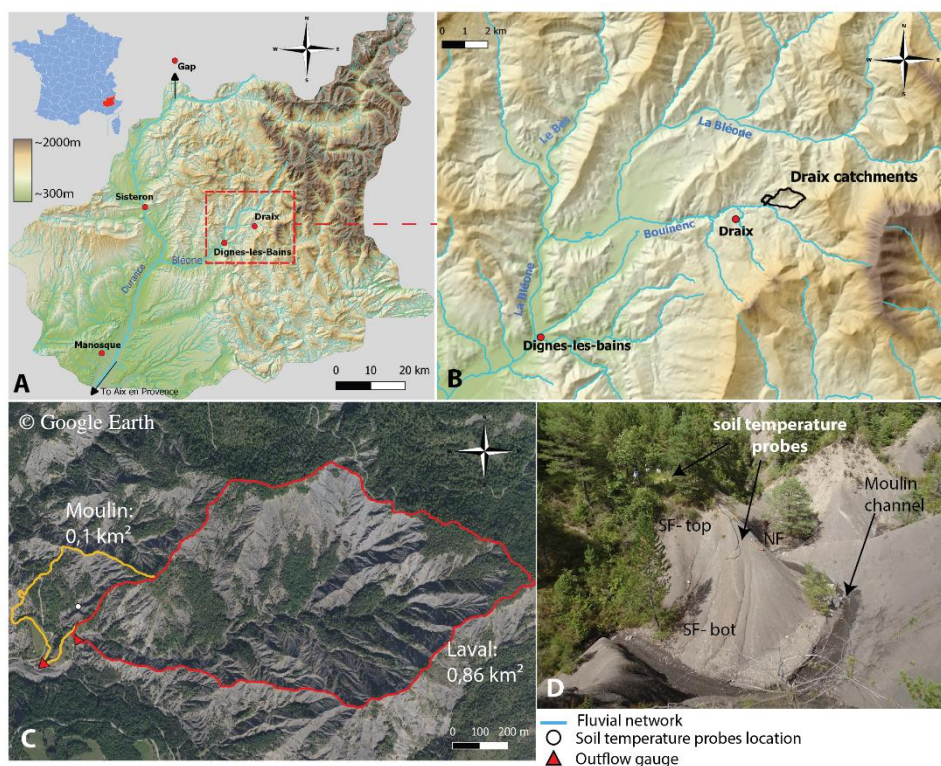
- Bechet, J., Duc, J., Loye, A., Jaboyedoff, M., Mathys, N., Malet, J.-P., Klotz, S., Le Bouteiller, C., Rudaz, B., and Travelletti, J.: Detection of seasonal cycles of erosion processes in a black marl gully from a time series of high-resolution digital elevation models (DEMs), *Earth Surf. Dynam.*, 4, 781–798, <https://doi.org/10.5194/esurf-4-781-2016>, 2016.
- 465 Brantley, S. L., Megonigal, J. P., Scatena, F. N., Balogh-Brunstad, Z., Barnes, R. T., Bruns, M. A., et al.: Twelve testable hypotheses on the geobiology of weathering. *Geobiology*, 9, 140–165, <https://doi.org/10.1111/j.1472-4669.2010.00264.x>, 2011.
- Buendia, C., Vericat, D., Batalla, R. J., and Gibbins, C. N.: Temporal dynamics of sediment transport and transient in-channel storage in a highly erodible catchment, *Land Degr. Devel.*, 27, 1045–1063, <https://doi.org/10.1002/ldr.2348>, 2016.
- 470 Carriere, A., Bouteiller, C. L., Tucker, G., Klotz, S., and Naaim, M.: Impact of vegetation on erosion: Insights from the calibration and test of a landscape evolution model in alpine badland catchments, *Earth Surf. Proc. Landf.*, 45, 1085–1099, <https://doi.org/10.1002/esp.4741>, 2020.
- Cheng, C.-L., Shalabh, and Garg, G.: Coefficient of determination for multiple measurement error models, *L. Multivar. Anal.*, 126, 137–152, <https://doi.org/10.1016/j.jmva.2014.01.006>, 2014.
- 475 Delannoy, J.-J. and Rovéra, G.: L'érosion dans les Alpes occidentales: Contribution à un bilan des mesures et des méthodes, *Rev. Geogr. Alp.*, 84, 87–101, 1996.
- Dixon, J. L., Heimsath, A. M., and Amundson, R.: The critical role of climate and saprolite weathering in landscape evolution, *Earth Surf. Proc. Landf.*, 34, 1507–1521, <https://doi.org/10.1002/esp.1836>, 2009.
- Draix-Bleone Observatory, Observatoire hydrosédimentaire de montagne Draix-Bléone [Data set]. Irstea.
- 480 <https://doi.org/10.17180/OBS.DRAIX>, 2015.
- Esteves, M., Descroix, L., Mathys, N., and Lapetite, J.M.: Soil hydraulic properties in a marly gully catchment (Draix, France), *CATENA*, 63, 282–298, <https://doi.org/10.1016/j.catena.2005.06.006>, 2005.
- Gaillardet, J., Braud, I., Hankard, F., Anquetin, S., Bour, O., Dorfliger, N., et al.: OZCAR: The French Network of Critical Zone Observatories, *Vad. Zone J.*, 17, 180067, <https://doi.org/10.2136/vzj2018.04.0067>, 2018.
- Giménez, R., Casali, J., Grande, I., Díez, J., Campo, M. A., Álvarez-Mozos, J., and Goñi, M.: Factors controlling sediment export in a small agricultural watershed in Navarre (Spain), *Agric. Wat. Manag.*, 110, 1–8, <https://doi.org/10.1016/j.agwat.2012.03.007>, 2012.
- 490 Hales, T. C. and Roering, J. J.: Climatic controls on frost cracking and implications for the evolution of bedrock landscapes, *J. Geophys. Res.*, 112, F02033, <https://doi.org/10.1029/2006JF000616>, 2007.
- Hallet, B., Walder, J. S., and Stubbs, C. W.: Weathering by segregation ice growth in microcracks at sustained subzero temperatures: Verification from an experimental study using acoustic emissions, *Permafr. Periglac. Process*, 2, 283–300, <https://doi.org/10.1002/ppp.3430020404>, 1991.
- Harvey, A.: Badland. In: Goudie, A.S. (Ed.), *Encyclopedia of Geomorphology*, Routledge, pp. 45–48, 2004.
- 495 Hirschberg, J., Fatichi, S., Bennett, G. L., McArdell, B. W., Peleg, N., Lane, S. N., Schlunegger, F., and Molnar, P.: Climate change impacts on sediment yield and debris-flow activity in an Alpine catchment, *J. Geophys. Res. Earth Surf.*, 126, e2020JF005739, <https://doi.org/10.1029/2020JF005739>, 2021.



- 500 Jantzi, H., Liébault, F., and Klotz, S.: Sediment residence time in alluvial storage of black marl badlands, *CATENA*, 156, 82–91, <https://doi.org/10.1016/j.catena.2017.03.026>, 2017.
- Klein, M.: Anti clockwise hysteresis in suspended sediment concentration during individual storms: Holbeck catchment; Yorkshire, England, *CATENA*, 11, 251–257, [https://doi.org/10.1016/0341-8162\(84\)90014-6](https://doi.org/10.1016/0341-8162(84)90014-6), 1984.
- Lana-Renault, N. and Regüés, D.: Bedload transport under different flow conditions in a human-disturbed catchment in the Central Spanish Pyrenees, *CATENA*, 71, 155–163, <https://doi.org/10.1016/j.catena.2006.04.029>, 2007.
- 505 Lemoine, M., Bas, T., Arnaud-Vanneau, A., Arnaud, H., Dumont, T., Gidon, M., et al.: The continental margin of the Mesozoic Tethys in the Western Alps, *Mar. Petrol. Geol.*, 3, 179–199, [https://doi.org/10.1016/0264-8172\(86\)90044-9](https://doi.org/10.1016/0264-8172(86)90044-9), 1986.
- Li, D., Overeem, I., Kettner, A. J., Zhou, Y., and Lu, X.: Air temperature regulates erodible landscape, water, and sediment fluxes in the permafrost-dominated catchment on the Tibetan Plateau, *Water Resour. Res.*, 57, <https://doi.org/10.1029/2020WR028193>, 2021.
- 510 Lickorish, W. H. and Ford, M.: Sequential restoration of the external Alpine Digne thrust system, SE France, constrained by kinematic data and synorogenic sediments, *Geol. Soc. Lond. Spec. Publ.*, 134, 189–211, <https://doi.org/10.1144/GSL.SP.1998.134.01.09>, 1998.
- Liébault, F.: Geomorphology and sediment transport of alpine fluvial systems: from steep-slope torrents to piedmont gravel-bed rivers, *Habil. Dir. Rech., Univ. Grenoble Alpes*, 150 pp., <https://hal.inrae.fr/tel-02606790>, 2017.
- 515 Mallet, F., Carrière, S.D., Chalikakis, K. and Marc, V.: Assessing soil water content spatio-temporal variability at the hillslope scale in a headwater catchment using a multi variable interpolation model based on EMI surveys (Draix, South Alps, France), *Env. Earth Sci.*, 77, 507, <https://doi.org/10.1007/s12665-018-7687-9>, 2018.
- Mathys, N.: Analyse et modélisation à différentes échelles des mécanismes d'érosion et de transport de matériaux solides. Cas des petits bassins versants de montagne sur marne (Draix, Alpes-de-Haute-Provence), Phd Thesis, INP Grenoble, 346 pp., <https://hal.inrae.fr/tel-02588905>, 2006.
- 520 Mathys, N., Brochot, S., Meunier, M., and Richard, D.: Erosion quantification in the small marly experimental catchments of Draix (Alpes de Haute Provence, France). Calibration of the ETC rainfall–runoff–erosion model, *CATENA*, 50, 527–548, [https://doi.org/10.1016/S0341-8162\(02\)00122-4](https://doi.org/10.1016/S0341-8162(02)00122-4), 2003.
- 525 Matsuoka, N.: Frost weathering and rockwall erosion in the southeastern Swiss Alps: Long-term (1994–2006) observations, *Geomorphology*, 99, 353–368, <https://doi.org/10.1016/j.geomorph.2007.11.013>, 2008.
- Matsuoka, N. and Murton, J.: Frost weathering: Recent advances and future directions, *Permafr. Periglac. Process*, 19, 195–210, <https://doi.org/10.1002/ppp.620>, 2008.
- 530 Nadal-Romero, E., Regüés, D., Martí-Bono, C., and Serrano-Muela, P.: Badland dynamics in the Central Pyrenees: temporal and spatial patterns of weathering processes, *Earth Surf. Proc. Landf.*, 32, 888–904, <https://doi.org/10.1002/esp.1458>, 2007.
- Nadal-Romero, E., Regüés, D., and Latron, J.: Relationships among rainfall, runoff, and suspended sediment in a small catchment with badlands, *CATENA*, 74, 127–136, <https://doi.org/10.1016/j.catena.2008.03.014>, 2008.
- Nadal-Romero, E., Martínez-Murillo, J. F., and Kuhn, N. J.: Badland dynamics in the context of global change, Elsevier, Amsterdam, Netherlands, 320 pp., 2018.

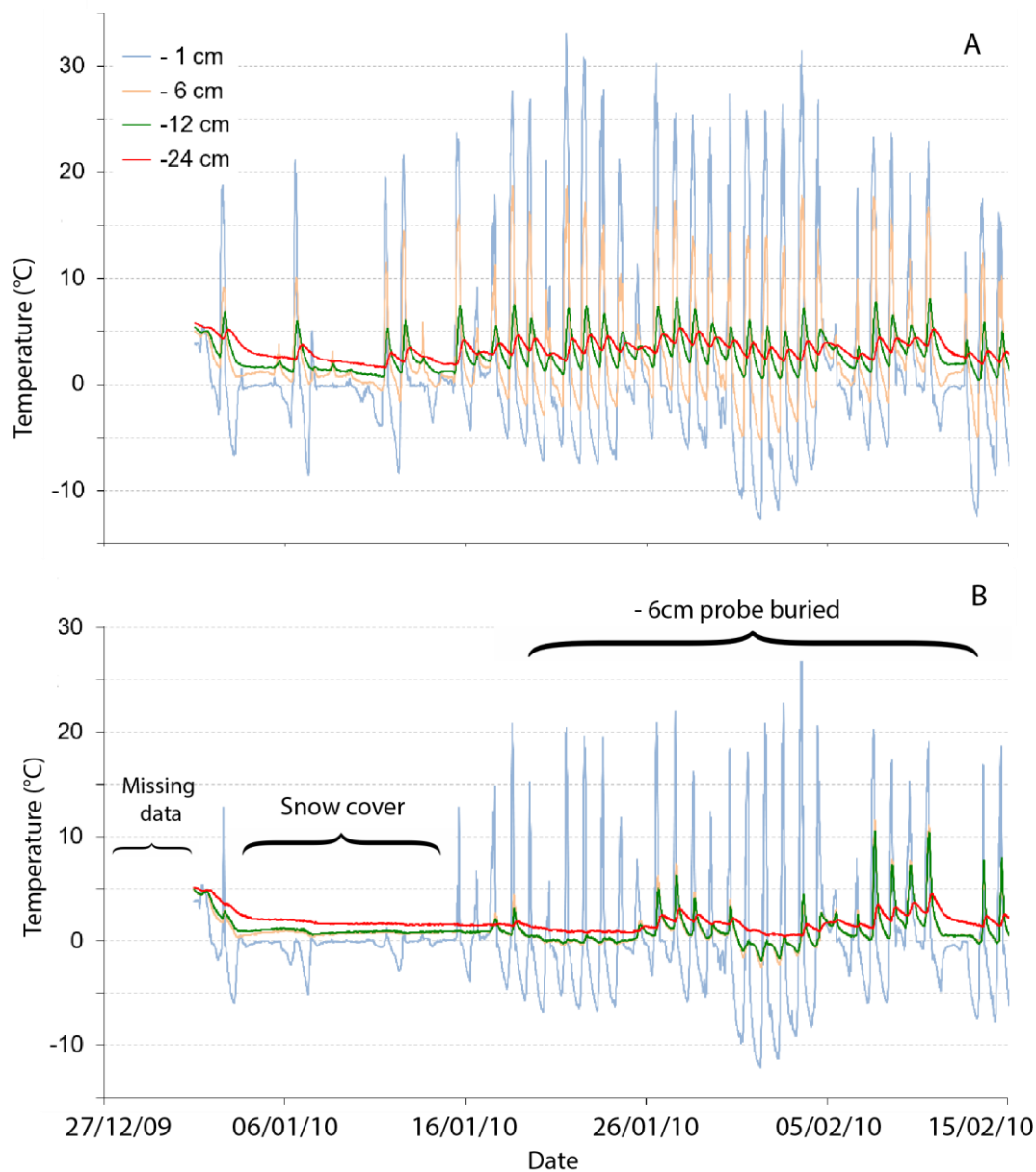


- 535 Nadal-Romero, E., Rodríguez-Caballero, E., Chamizo, S., Juez, C., Cantón, Y., and García-Ruiz, J. M.: Mediterranean badlands: Their driving processes and climate change futures, *Earth Surf. Proc. Landf.*, in press, <https://doi.org/10.1002/esp.5088>, 2021.
- Nearing, M. A., Pruski, F. F., and O’Neal, M. R.: Expected climate change impacts on soil erosion rates: A review, *J. Soil Wat. Conserv.*, 59, 43–50, 2004.
- 540 Rainato, R., Mao, L., García-Rama, A., Picco, L., Cesca, M., Vianello, A., Preciso, E., Scussel, G. R., and Lenzi, M. A.: Three decades of monitoring in the Rio Cordon instrumented basin: Sediment budget and temporal trend of sediment yield, *Geomorphology*, 291, 45–56, <https://doi.org/10.1016/j.geomorph.2016.03.012>, 2017.
- Regüés, D., Pardini, G., and Gallart, F.: Regolith behaviour and physical weathering of clayey mudrock as dependent on seasonal weather conditions in a badland area at Vallcebre, Eastern Pyrenees, *CATENA*, 25, 199–212, [https://doi.org/10.1016/0341-8162\(95\)00010-P](https://doi.org/10.1016/0341-8162(95)00010-P), 1995.
- 545 Rengers, F. K., Kean, J. W., Reitman, N. G., Smith, J. B., Coe, J. A., and McGuire, L. A.: The influence of frost weathering on debris flow sediment supply in an Alpine basin, *J. Geophys. Res. Earth Surf.*, 125, e2019JF005369, <https://doi.org/10.1029/2019JF005369>, 2020.
- Riebe, C. S., Hahm, W. J., and Brantley, S. L.: Controls on deep critical zone architecture: a historical review and four testable hypotheses, *Earth Surf. Proc. Landf.*, 42, 128–156, <https://doi.org/10.1002/esp.4052>, 2017.
- 550 Rovéra, G. and Robert, Y.: Conditions climatiques hivernales et processus d’érosion périglaciaires dans les bad-lands marneux de Draix (800 m, Alpes du Sud, France), *Géogr. Phys. Quat.*, 59, 31–48, <https://doi.org/10.7202/013735ar>, 2005.
- Tolorza, V., Carretier, S., Andermann, C., Ortega-Culaciati, F., Pinto, L., and Mardones, M.: Contrasting mountain and piedmont dynamics of sediment discharge associated with groundwater storage variation in the Biobío River, *J. Geophys. Res. Earth Surf.*, 119, 2730–2753, <https://doi.org/10.1002/2014JF003105>, 2014.
- 555 West, A. J., Galy, A., and Bickle, M.: Tectonic and climatic controls on silicate weathering. *Earth Planet. Sci. Lett.*, 235, 211–228, <https://doi.org/10.1016/j.epsl.2005.03.020>, 2005.
- 560 York, D., Evensen, N. M., Martínez, M. L., and De Basabe Delgado, J.: Unified equations for the slope, intercept, and standard errors of the best straight line, *Am. J. Phys.*, 72, 367–375, <https://doi.org/10.1119/1.1632486>, 2004.

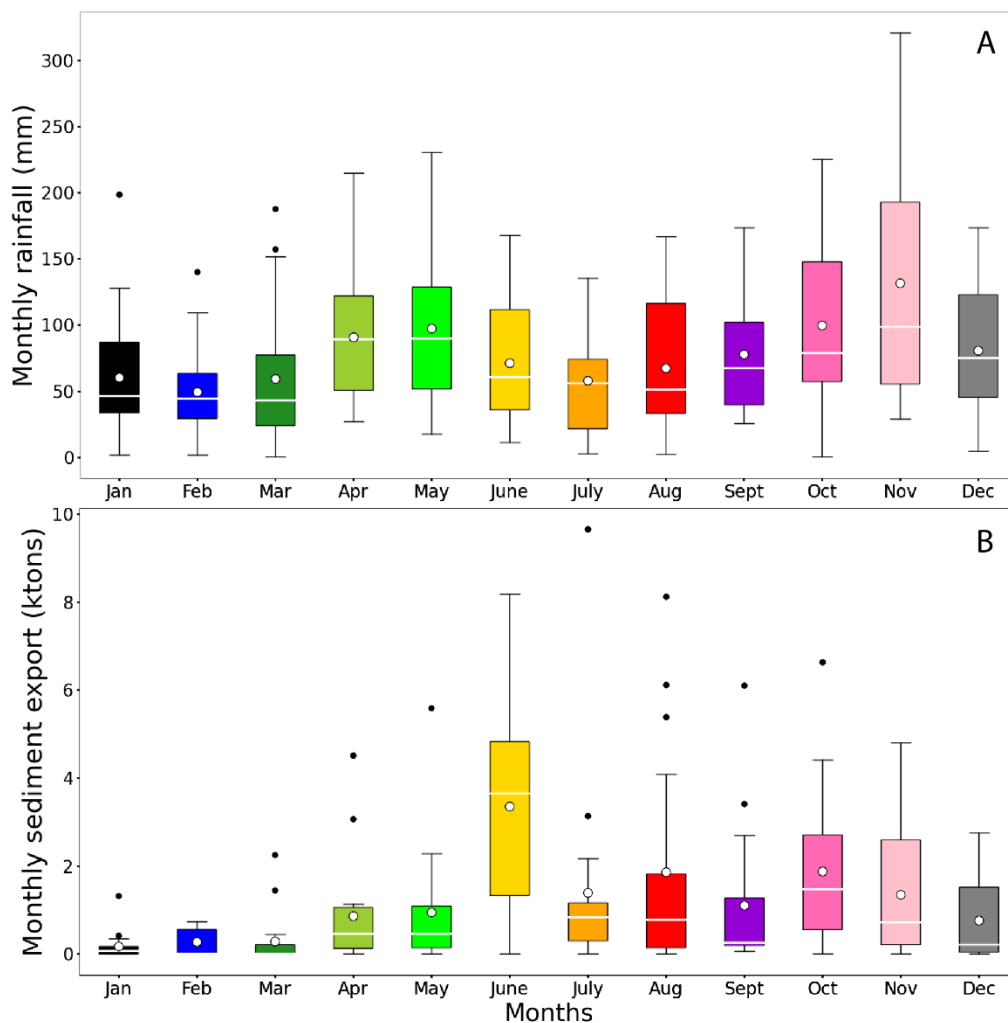


565

**Figure 1: Geographic setting of Draix-Bléone Critical Zone Observatory. (A) Digital Elevation Model (Institut Géographique National RGEAlti-50 m) of the 'Alpes de Hautes-Provence' department of southeast France, red box shows location of B; (B) Zoom on the Bouinenc catchment, black outlines show Moulin and Laval catchments. (C) Satellite image (from Google Earth) of the Moulin and Laval catchments, showing location of outflow gauges and soil-temperature probes. (D) Setting of soil-temperature measurement sites, in a meander of the Moulin stream on north-facing (NF) and south-facing (SF) slopes at different locations (uphill and downhill) on the hillslopes.**



570 **Figure 2: (A) Typical soil-temperature series recorded with four probes at different depths (from south-facing downhill location). (B) Example of soil-temperature series (from north-facing uphill location) biased because of climatic conditions (snow cover), buried or loosened probes.**



575 **Figure 3: Boxplots of (A) monthly rainfall and (B) monthly total sediment export (i.e., bedload + suspended load) of the Laval catchment. White line shows median value and white dot indicates mean value. The first (Q1, 25%) and third (Q3 75%) percentiles are indicated by the box limits, whiskers show  $Q1 - 1.5 * IQR$  and  $Q3 + 1.5 * IQR$  (inter-quartile range). Black dots are outlier values.**

580



585

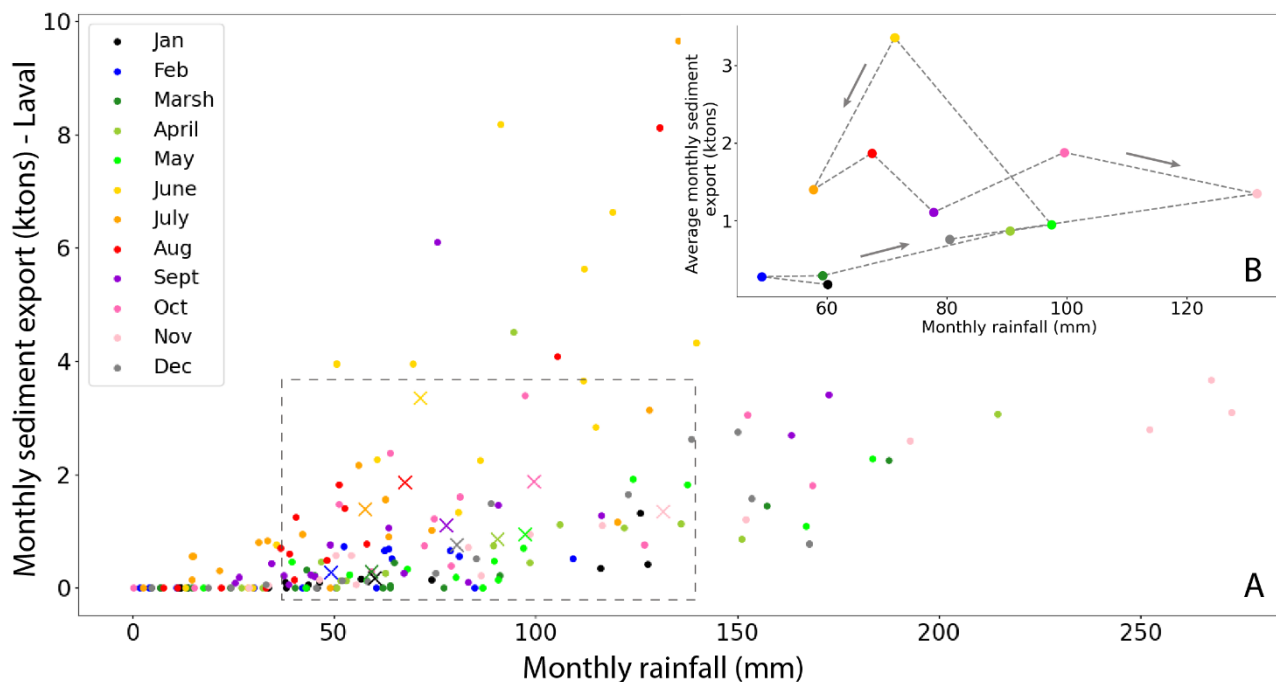
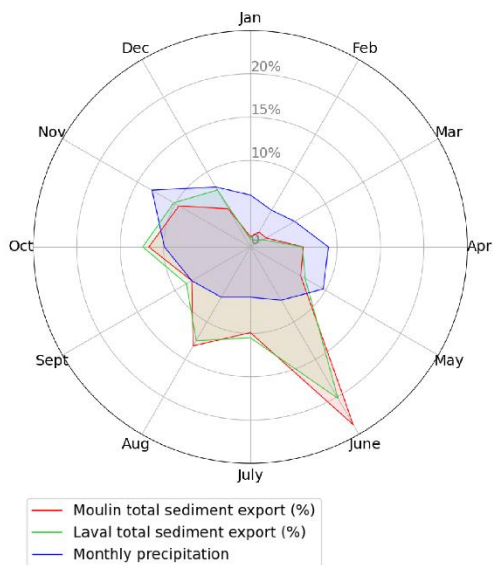


**Figure 4: Monthly sediment export (ktons) from the Laval catchment versus monthly rainfall between 2003 and 2019. (A) Individual values for each month (dots) and interannual monthly averages (crosses) over the analysed period. Dashed box shows limits of inset (B). (B) Hysteresis plot using interannual monthly average values. Dashed line highlights the hysteresis cycle with two separate maxima: high sediment export and moderate rainfall in June versus high total rainfall and moderate sediment export in October/November**



590 **Figure 5: Comparison of the relative distribution of monthly sediment export for the Laval and Moulin catchments, together with relative monthly rainfall distribution.**

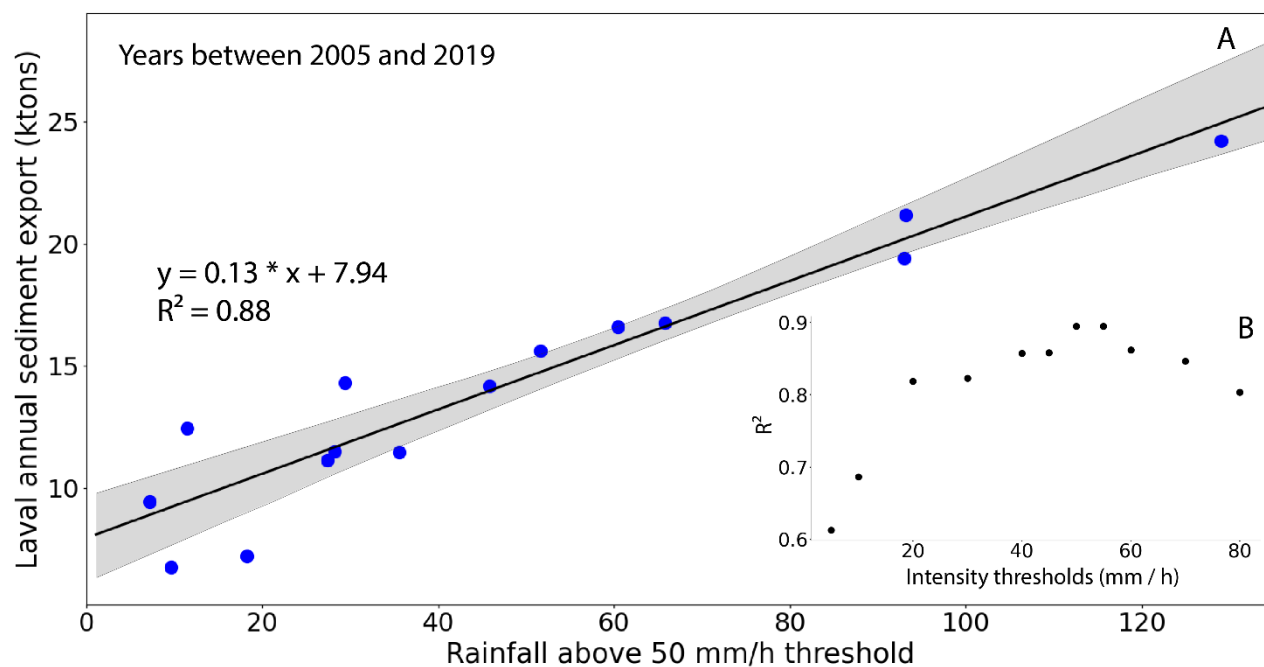
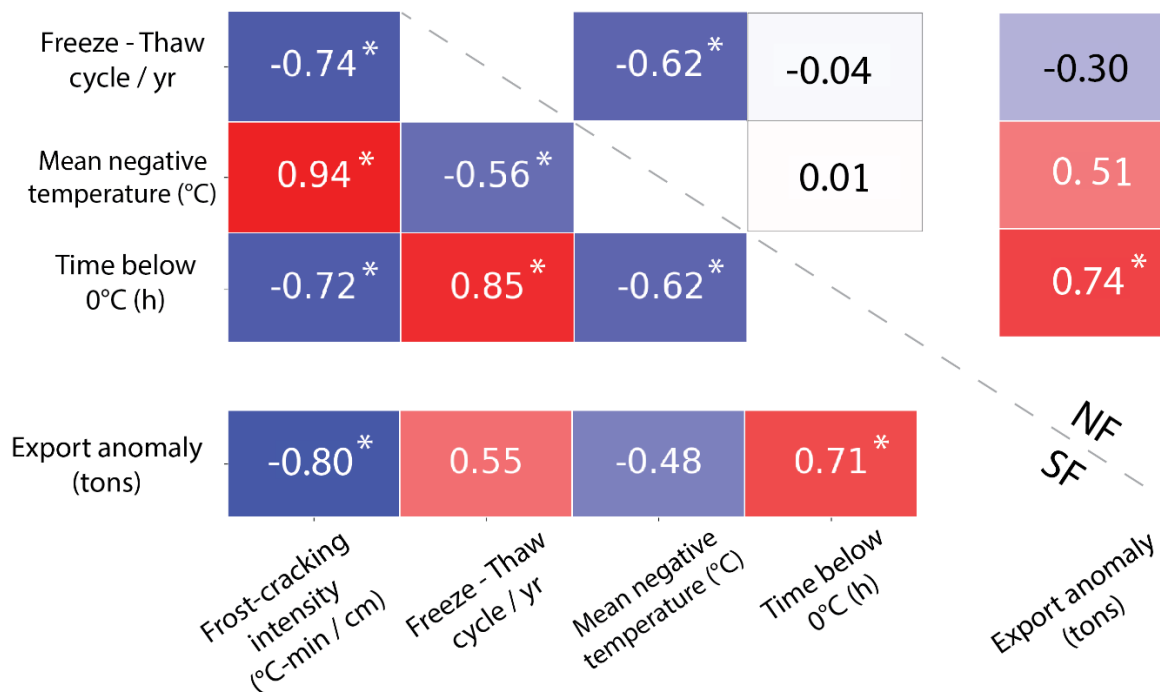


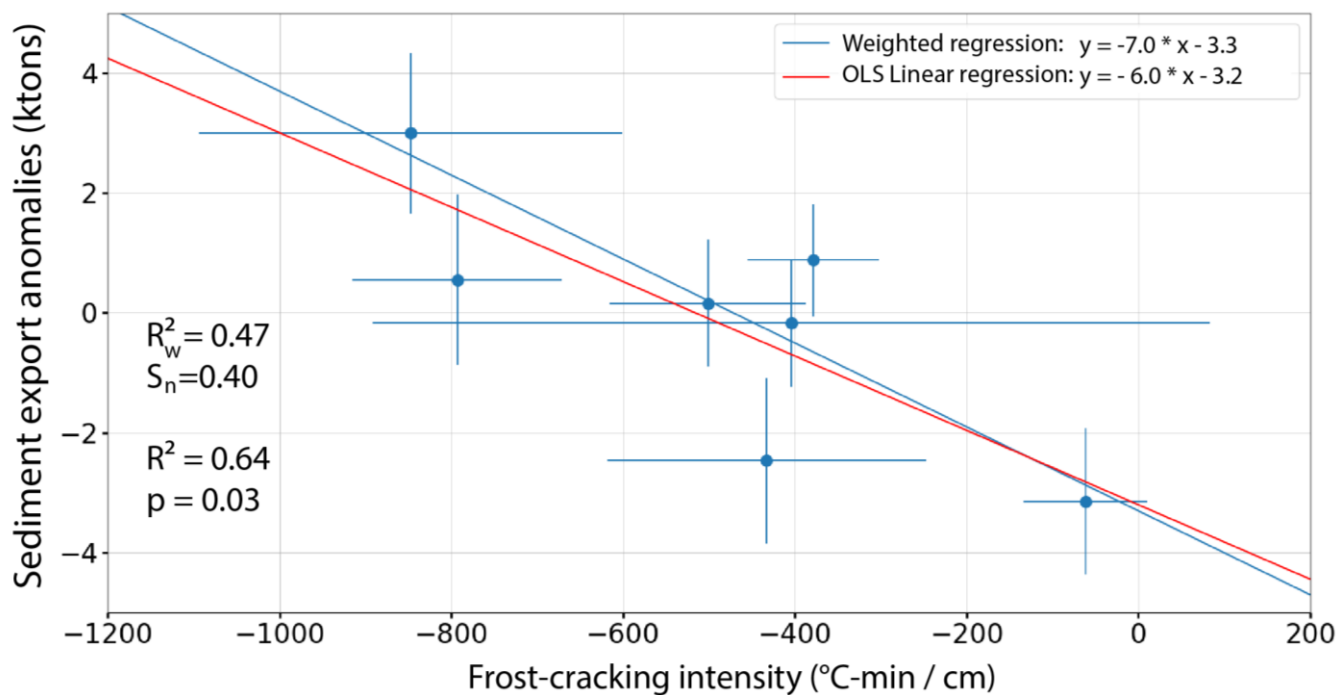
**Figure 6: (A) Linear correlation between annual total sediment export from the Laval catchment and rainfall above a threshold of 50 mm/h for the years 2005 to 2019 (blue dots). Regression line is in black; grey shaded area shows 95% confidence interval. Most outliers occur for low cumulative rainfall above the threshold (< 40 mm). (B) Coefficient of determination ( $R^2$ ) between annual sediment export and annual rainfall above threshold for different intensity thresholds. Optimum correlations are found for threshold values between 50 and 55 mm/h.**

595

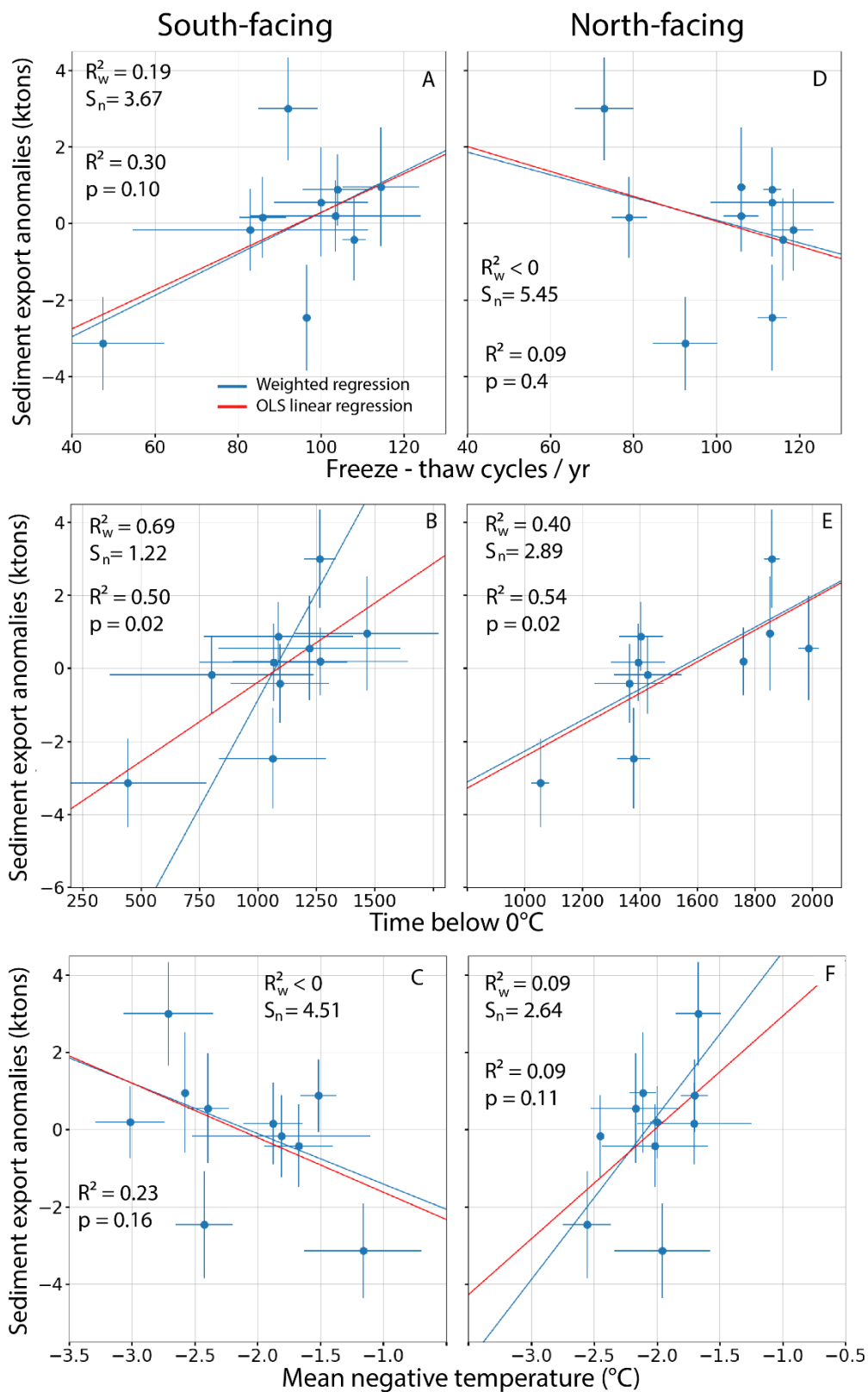


600 **Figure 7: Correlation matrix between different soil-temperature indicators computed from all data points (using both uphill and downhill locations on the same slope); and between soil-temperature indicators and sediment-export anomaly (calculated using averages between uphill and downhill locations from the same slope). Lower-left and upper-right parts of the table report correlations for south-facing (SF) and north-facing (NF) slopes, respectively. Blue boxes show negative correlations and red boxes show positive correlations; values indicate correlation coefficient R and stars (\*) indicate significant correlations (i.e.,  $p < 0.05$ ).**

605



610 Figure 8: Regression analysis between sediment-export anomalies and frost-cracking intensity on the south-facing slope for the years  
2007, 2008, 2009, 2010, 2014, 2015 and 2017. Horizontal error bars refer to the difference between measurements at uphill and  
downhill locations (temperature measurements for 2017 were only available for the downhill location, thus uncertainty on frost-  
cracking intensity was computed as the average of the uncertainties from the others years); vertical error bars are  $\pm 2\sigma$  uncertainty  
in export anomaly. Red line shows ordinary least-squares (OLS) linear regression whereas blue line shows weighted linear regression  
615 following York et al. (2004). Weighted determination coefficients  $R_w^2$  and associated normalized goodness-of-fit indicator  $S_n = S /$   
(n-2) are indicated for the weighted regression. Standard  $R^2$  and associated p-value indicate significance of the ordinary least-squares  
(unweighted) regression.





620

**Figure 9: Linear regression analysis between sediment-export anomalies and (A-D) number of freeze-thaw cycles per year; (B-E) time spent below 0 °C; and (C-F) mean negative temperature. Left column shows regressions for south-facing slope and right column for north-facing slope. Error bars and red and blue regression lines are as in Figure 8. Weighted determination coefficients  $R^2_w$  and associated normalized goodness of fit indicators  $S_n$  are indicated for each weighted regression. Standard  $R^2$  and associated p-value indicate significance of the ordinary least-squares (unweighted) regressions.**